Available online at www.sciencedirect.com
SCIENCE DIRECT®
Geochimica et Cosmochimica Acta 70 (2006) 290–305
Geochimica
www.elsevier.com/locate/gca

The effect of $Al(OH)_4^-$ on the dissolution rate of quartz

Barry R. Bickmore [a,*], Kathryn L. Nagy [b], Amy K. Gray [c], A. Riley Brinkerhoff [d]

[a] Department of Geology, Brigham Young University, Provo, UT 84602-4606, USA
[b] Department of Earth and Environmental Sciences, University of Illinois at Chicago (MC-186), 845 West Taylor Street, Chicago, IL 60607-7059, USA
[c] Department of Geosciences, College of Natural Resources, Colorado State University, Fort Collins, CO 80523-1482, USA
[d] Department of Geology, Brigham Young University, Provo, UT 84602, USA

Received 13 April 2005; accepted in revised form 20 September 2005

Abstract

The influence of $Al(OH)_4^-$ on the dissolution rate of quartz at pH 10–13 and 59–89 °C was determined using batch experiments. $Al(OH)_4^-$ at concentrations below gibbsite solubility depressed the dissolution rate by as much as 85%, and this effect was greater at lower pH and higher $Al(OH)_4^-$ concentration. Dissolution rates increased with increasing temperature; however, the percent decrease in rate due to the presence of $Al(OH)_4^-$ was invariant with temperature for a given H^+ activity and $Al(OH)_4^-$ concentration. These data, along with what is known about Al–Si interactions at high pH, are consistent with $Al(OH)_4^-$ and Na^+ co-adsorbing on silanol sites and passivating the surrounding quartz surface. The observed pH dependence, and lack of temperature dependence, of inferred $Al(OH)_4^-$ sorption also supports the assumption that the acid–base behavior of the surface silanol groups has only a small temperature dependence in this range. A Langmuir-type adsorption model was used to express the degree of rate depression for a given in situ pH and $Al(OH)_4^-$ concentration. Incorporation of the rate data in the absence of aluminate into models that assume a first-order dependence of the rate on the fraction of deprotonated silanol sites was unsuccessful. However, the data are consistent with the hypothesis proposed in the literature that two dissolution mechanisms may be operative in alkaline solutions: nucleophilic attack of water on siloxane bonds catalyzed by the presence of a deprotonated silanol group and OH^- attack catalyzed by the presence of a neutral silanol group. The data support the dominance of the second mechanism at higher pH and temperature.

1. Introduction

Silicate mineral dissolution rates have not been studied as systematically in highly alkaline solutions as under the mildly acidic to neutral pH range more typical of natural weathering. In fact, weathering of alkaline igneous rocks can result in groundwaters with pH values as high as 11 (Drever, 1997), and, there is a growing need for rate information in compositionally complex, basic solutions due to the extreme conditions produced in certain engineered systems, such as nuclear waste facilities and oil fields. Many proposed nuclear waste storage facilities have engineered barrier systems that include grouts or cements that would equilibrate with ambient pore waters at pH values of 12 or higher (e.g., Hoch et al., 2004). Alkaline flooding of petroleum reservoirs enhances recovery by reducing the interfacial tension of oil using a combination of basic reagents and surfactants (Hornof et al., 2000). Reaction of the alkalis with reservoir minerals between the injection and production wells (e.g., Labrid and Duquerroix, 1991; Bagci et al., 2000) can alter porosity and permeability over the flooding path, and hence the extent of recovery.

A pressing example of a situation in which detailed understanding of silicate dissolution rates at high pH is needed is at the US Department of Energy's Hanford Site in southeast Washington where reprocessing of spent nuclear fuel has created enormous volumes of radioactive waste in extreme chemical environments. The pH of this complex waste was raised by the addition of sodium hydroxide before storing in underground carbon steel tanks. Precipitation, self-boiling, and waste concentration

* Corresponding author. Fax: +1 801 422 0267.
E-mail address: barry_bickmore@byu.edu (B.R. Bickmore).

0016-7037/$ - see front matter © 2005 Elsevier Inc. All rights reserved.
doi:10.1016/j.gca.2005.09.017

procedures reduced the liquid volume in the tanks over time, often resulting in high-aluminum, high-pH (9–14), high-ionic-strength, high-temperature slurries (Gephart and Lundgren, 1998). The tanks have leaked 0.6–1.4 million gallons of waste containing an estimated 1–2 million curies of radiation, primarily from ^{137}Cs into the underlying sediments since the late 1950s (Gephart and Lundgren, 1998).

Recent investigations of Hanford sediment samples from beneath two tank farms have discovered that dissolution of primary minerals by leaked waste solutions has affected the mobility of radionuclide and toxic contaminants. Chromate has been immobilized as both Cr(III) and Cr(VI) solid phases at the S-SX tank farm (Zachara et al., 2004), and a likely reductant was Fe(II) dissolved from biotite and vermiculite based on the observed association of Cr(III) with these primary minerals in core samples and experimental data (Qafoku et al., 2003; He et al., 2005; Samson et al., 2005). Secondary precipitates apparently zeolitic in composition and presumably sequestering ^{137}Cs also were observed on quartz and other aluminosilicate clasts within 5 m of the tanks at the same site (Zachara et al., 2004). Uranium-silicate secondary precipitates were observed in association with plagioclase feldspar beneath the BX tank farm (Catalano et al., 2004), and it was surmised that the source of Si in the precipitates was from dissolution of the feldspar. Zeolitic phases such as cancrinite and sodalite form easily in the laboratory by the interaction of quartz (Bickmore et al., 2001), kaolinite (Chorover et al., 2003; Zhao et al., 2004), and both simulated and real Hanford sediments in batch reactor and column experiments (Nyman et al., 2000; Mashal et al., 2004; Qafoku et al., 2003, 2004; Wan et al., 2004). Dissolution of primary minerals in Hanford sediments can result in both colloidal secondary precipitates as well as heterogeneously nucleated phases. The first type of precipitate may enhance contaminant mobility as shown by experimentation (Flury et al., 2002; Zhuang et al., 2003; Cherrey et al., 2003) and the second may retard contaminant transport as indicated from the field samples. Both could affect permeability and subsequent flow paths of groundwater or waste solutions.

In these many examples of natural and manmade high pH environments that exist in the subsurface, little is known about the effect of dissolved aluminum on the dissolution rates of silicate minerals. Because aluminum solubility increases with increasing pH in the basic region, its influence on dissolution rates will be important, whether or not the aluminum is derived from natural dissolution processes or by artificial addition, as in the Hanford Site case. At ambient temperatures, dissolved aluminum suppresses feldspar dissolution under acidic conditions (Chou and Wollast, 1985; Oelkers et al., 1994) and has variable effects on biotite dissolution rates at basic pH values (Samson et al., 2005). A number of workers (Liefländer and Stöber, 1960; Lewin, 1961; Jones and Handreck, 1963; Hingston and Raupach, 1967; Ballou et al., 1973; Iler, 1973; Van Bennekom et al., 1991; Van Cappellen and Qiu, 1997a,b) have observed that sorbed Al species depress silica (e.g., quartz or metastable silica phases) dissolution rates in mildly alkaline solutions, and in fact may lower silica solubility by creating a new aluminosilicate surface phase, even at fractional surface coverage. However, these investigations on silica phases were largely qualitative, and Dove (1995) noted that it was unclear whether Al had any effect at concentrations undersaturated with respect to Al-oxyhydroxides.

We report the results of batch experiments designed to measure the dissolution kinetics of quartz sand in high pH solutions with varying Al and $NaNO_3$ concentrations at 59, 75, and 89 °C. These results are then analyzed in terms of possible molecular-scale mechanisms for quartz dissolution at high pH in general and for the specific effects of Al solution species on quartz dissolution rates.

2. Materials and methods

2.1. Materials

White quartz sand (Aldrich) used in the experiments was 99.8% SiO_2 according to X-ray fluorescence (XRF) analysis. Minor mineral impurities were visible in an optical microscope, but could not be detected with powder X-ray diffraction (XRD). Magnetic impurities were removed from the sand sample by magnetic separation, after which 300 g of sand were reacted with 400 mL concentrated H_2SO_4 in a glass bottle for 2 days. The treated sample was rinsed gently 5–10 times and then soaked at 75 °C in 2 L of doubly deionized (DDI) water for 3 days, changing the water every day. Again the sand was rinsed gently 5–10 times and finally dried at 80 °C. Auger electron spectroscopy (AES) of untreated quartz surfaces with a Perkin–Elmer PHI 600 Scanning Auger Multiprobe revealed no surface impurities except adventitious C and trace Ca, perhaps from $CaCO_3$. AES spectra of treated quartz surfaces revealed no impurities other than adventitious C. XRF analysis of the treated sample showed that it was 99.9% SiO_2.

Digital reflected light microscopy images were taken of the sand grains and the specific surface area (SSA) was estimated by image analysis. The cross-sectional area of 38 grains was calculated using NIH Image (Rasband and Bright, 1995), and an "average diameter" assigned assuming a circular shape. The SSA was calculated by assuming the volume and twice the surface area of a sphere of the same diameter to account for the contribution from surface roughness. The cumulative SSA for the grains analyzed was 0.013 m^2/g. The sand grains were quite uniform in size; "average diameters" ranged from 260 to 474 μm with a mean of 344 ± 14 μm (95% confidence interval).

Solutions were prepared using reagent grade NaOH, $NaNO_3$, and $Al(NO_3)_3$. DDI water (18.2 MΩ, Barnstead Nanopure deionization system) was boiled and simultaneously purged with Ar(g), then stored in collapsible plastic containers with no headspace. Ar(g) was again bubbled

through each solution as the reagents were mixed in the order: NaOH, $Al(NO_3)_3$, and $NaNO_3$. Solutions were immediately poured into the reaction vessels and sealed, with minimal headspace.

2.2. Batch dissolution experiments

Sixty batch experiments were designed to measure quartz dissolution. Solutions were made with 0–4 m $NaNO_3$, 0.0000, 0.0001, 0.001, 0.005, or 0.01 m $Al(NO_3)_3$, and enough NaOH to account for the formation of $Al(OH)_4^-$ and create free OH^- concentrations of 0.001, 0.004, 0.01, 0.1, or 1.0 m (Table A1). One to three grams of treated quartz sand were placed in each of eight HDPE plastic bottles (60 mL), which were filled with solution. Bottles were placed in a constant temperature bath (59, 75, or 89 °C), and one bottle at a time was removed for analysis. To avoid abrasion of the quartz surfaces, the bottles were not shaken. The pH of each sample was measured (see below), and 25 mL aliquots of the solution were acidified with either 0.25 mL of 12.1 M HCl for Al analysis or 0.06 mL of 4.5 M H_2SO_4 for Si analysis. These solutions were analyzed for Al (error ± 7%) and Si (error ± 5%) concentration using colorimetry (Dougan and Wilson, 1974; Koroleff, 1983) or inductively coupled plasma atomic emission spectroscopy (ICP-AES) (error ± 3%). A Bausch & Lomb Spectronic 501 spectrophotometer was used for the colorimetric analyses and a Fisons Instruments ARL 3410+ for ICP-AES.

Initial quartz dissolution rates were calculated because at elevated dissolved Si concentrations, some solutions precipitated nitrate–cancrinite, a zeolite-like aluminosilicate (Bickmore et al., 2001). Si release data collected in solutions with 2 m $NaNO_3$ were used to quantify the effect of $Al(OH)_4^-$ on the quartz dissolution rate. Errors in the rate calculations were estimated at ±15% in all cases. Solution data for all samples are tabulated in electronic annex EA-1.

2.3. pH measurement

Upon removal from the bath, each sample bottle was opened and partially immersed in a beaker of the hot bath water for pH measurement at a temperature near that of the bath. Solution pH was measured with an Accumet AR-15 pH meter (Fisher) and AccuFet (Fisher) solid state ion sensitive field effect transistor (ISFET) electrode with automatic temperature correction. The temperature dependence of the equilibrium constant for the dissociation of water was then used to correct the measured pH to the bath temperature. The pH was measured at high temperature to minimize the amount of dissolved CO_2, which caused the pH to drift downward as the solution cooled. ISFET electrodes eliminate Na^+ error, caused by Na^+ ions migrating through the gel layer of a glass electrode (McMillan, 1991; McMillan, 1993).

Solution pH calculated using the equilibrium model described below differed from the temperature-corrected measured values by up to +0.3 pH units. For the purpose of solubility estimations and rationalization of dissolution rates it was assumed that the modeled values were more accurate. Measurements were made only to confirm that the pH did not drift significantly during the experiments. The discrepancy between measured and calculated pH can be traced to the following possible causes. First, pH 10.00 (Fisher) and 13.00 (Bates, 1964) buffers were used to calibrate the electrode at room temperature. The pH 13.00 buffer is prone to pH drift (McMillan, 1991), and the buffers do not bracket the experimental solution conditions. Second, the temperature sensor was imbedded within the electrode in this case, and this can result in slow temperature compensation response and measurement errors (McMillan, 1991). (It should also be noted that the standardization of the electrode at room temperature could have been problematic.) Third, changes in activity coefficients, etc., due to large differences in ionic strength between the buffers and samples can lead to errors, as well (Stumm and Morgan, 1996).

2.4. Solution model

The *Geochemist's Workbench* 3.0 (GWB) (Bethke, 1998) was used to model solution speciation. Equilibrium constants were used as given in the GWB database, except those for dissolved Al species and gibbsite, which were taken from Wesolowski (1992), and that for the polysilicate species $Si_4(OH)_{18}^{2-}$, taken from Busey and Mesmer (1977). Several polynuclear silicate species are known to exist in solution (Sjöberg et al., 1985), but Busey and Mesmer (1977) assumed only one, using it to represent all polysilicate species. We have followed Busey and Mesmer (1977) because we know of no other thermodynamic data for polysilicate equilibria above 25 °C.

Due to the high ionic strengths used, the Pitzer model capability of GWB was implemented with interaction parameters taken from the literature (Table 1).

Care was taken to ensure that none of the solutions used in the experiments were saturated with respect to gibbsite or boehmite. The GWB Pitzer model used predicts that gibbsite is the more stable solid phase under the conditions studied. Calculated solubilities of gibbsite in 2 m $NaNO_3$ at 59, 75, and 89 °C over the alkaline pH range are plotted along with the solution conditions of our 2 m $NaNO_3$ experiments in Fig. 1.

2.5. Adsorption model

It was assumed that the depression of the quartz dissolution rate in the presence of $Al(OH)_4^-$ was due to poisoning of the surface by specific adsorption and was proportional to the fraction of surface sites covered. Two approaches were used to model the adsorption of $Al(OH)_4^-$ on the quartz surface, and hence the depression of the dissolution rate. First, an attempt was made to extend the triple layer model (TLM) proposed by Dove (1994) to include $Al(OH)_4^-$ adsorption.

Table 1
Pitzer parameters used in our solution equilibrium calculations, along with temperature correction factors,[a] where available

	Value	c_1	c_2
Na^+–OH^- (GWB database)			
β^0	0.0864	7.00×10^{-4}	
β^1	0.253	1.34×10^{-4}	
C^Φ	0.0044	-1.894×10^{-5}	
α	2.0		
Na^+–NO_3^- (Pitzer, 1991)			
β^0	6.8×10^{-3}	1.266×10^{-3}	
β^1	1.783×10^{-1}	2.06×10^{-3}	
C^Φ	-7.2×10^{-4}	-2.316×10^{-4}	
α	2.0		
Na^+–$Al(OH)_4^-$ (Wesolowski, 1992)			
β^0	4.50×10^{-2}	-1.9122×10^{-3}	−220.11059
β^1	3.1×10^{-1}	-3.7109×10^{-3}	−435.35236
C^Φ	-3×10^{-4}	2.4639×10^{-4}	34.9371858
α	2.0		
Na^+– H_4SiO_4 (Azaroual et al., 1997)			
λ	9.25×10^{-2}		
NO_3^-–H_4SiO_4 (Azaroual et al., 1997)			
λ	-9.4×10^{-3}		
Na^+– H_3SiO4^- (Hershey and Millero, 1986)			
β^0	4.30×10^{-2}	-1.9122×10^{-3}	−220.11059
β^1	2.4×10^{-1}	-3.7109×10^{-3}	−435.35236
C^Φ	0		
α	2.0		
Na^+– H_2SiO4^{2-} (Hershey and Millero, 1986)			
β^0	3.2×10^{-1}		
β^1	1.3×10^{-1}		
C^Φ	0		
α	2.0		
Na^+–$Si_4(OH)_{18}^{2-}$ (Pitzer, 1991)[b]			
β^0	-5.83×10^{-2}		
β^1	1.4655		
C^Φ	1.47×10^{-2}		
α	2.0		

[a] The c_1 and c_2 values are constants used to correct Pitzer model parameters (P) for temperature (T) using the following equation:

$$P = P_r + c_1(T_K - T_r) + c_2\left(\frac{1}{T_K} - \frac{1}{T_r}\right),$$

where T_r=298.15 K and P_r is the parameter value at T_r.

[b] These parameters are taken from Pitzer (1991) for the Na^+–HPO_4^{2-} interaction, which Wanner and Forest (1992) suggested as a proxy for Na^+ interactions with divalent polysilicic acid species.

The programs HYDRAQL (Papelis et al., 1988) and FITEQL 2.0 were used to reproduce Dove's TLM, as well as that proposed by Kent et al. (1988). The second approach was to describe the adsorption reaction as a simple Langmuir isotherm (Langmuir, 1997).

3. Results

3.1. Baseline dissolution rates

Quartz dissolution rates in Al-free solutions agree well, both in magnitude and pH dependence, with those reported in the literature for similar temperature and pH conditions (Brady and Walther, 1990; Knauss and Wolery, 1988; Schwartzentruber et al., 1987), although our experiments extend to higher pH (Fig. 2).

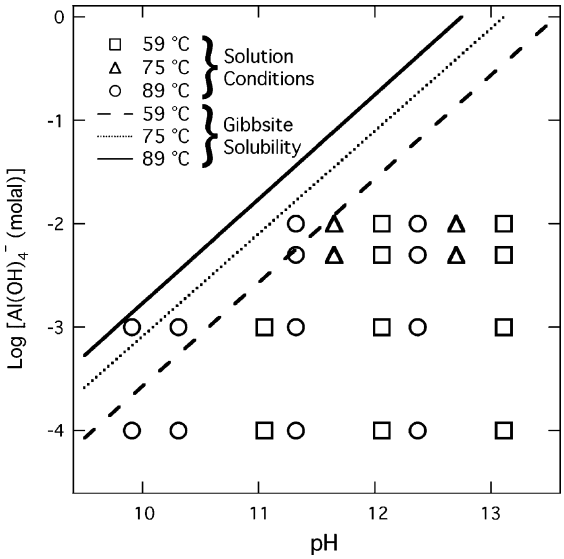

Fig. 1. Lines represent the solubility of gibbsite with 2 m $NaNO_3$ present at 59, 75, and 89 °C, as calculated with the Pitzer model described in the text. Symbols represent the conditions of the 2 m $NaNO_3$ experimental solutions. All solutions were undersaturated with respect to gibbsite, the most stable Al-oxyhydroxide under these conditions.

The data at 89 °C include solutions with 0 and 2 m $NaNO_3$. There is no measurable effect of $NaNO_3$ concentration under these conditions, since all the solutions had some Na^+ from the addition of NaOH (House, 1994; Dove, 1994).

Linear regressions of the baseline rates (R_B) at 59, 75, and 89 °C with respect to pH, and subsequent regression of the slopes and intercepts of these lines with respect to temperature (°C), produced the following empirical rate equation, where the pH is at temperature and the parenthetical error estimate is the standard error:

$$\mathrm{Log}[R_B(\mathrm{mol/m^2\ s})](\pm0.14) = (0.0113T - 0.499)\mathrm{pH} - 0.0919T - 5.19. \quad (1)$$

3.2. Effect of $Al(OH)_4^-$

Quartz dissolution rates in solutions containing dissolved aluminum were significantly depressed with increasing $Al(OH)_4^-$ concentration, but did not vary within error with Na^+ concentration. For example, at 0.005 m $Al(OH)_4^-$, 89 °C, and 0.1 m free OH^- there is no clear trend in the rates with Na^+ concentration or ionic strength for 0, 0.5, 1.0, 2.0, and 4.0 m $NaNO_3$ solutions, except perhaps at $NaNO_3$ concentrations below 1.0 m (Fig. 3). However, there is a consistent trend of depression of the dissolution rates in the entire dataset with increasing $Al(OH)_4^-$ concentration (Figs. 3 and 4). At higher $Al(OH)_4^-$ concentrations the degree of rate depression

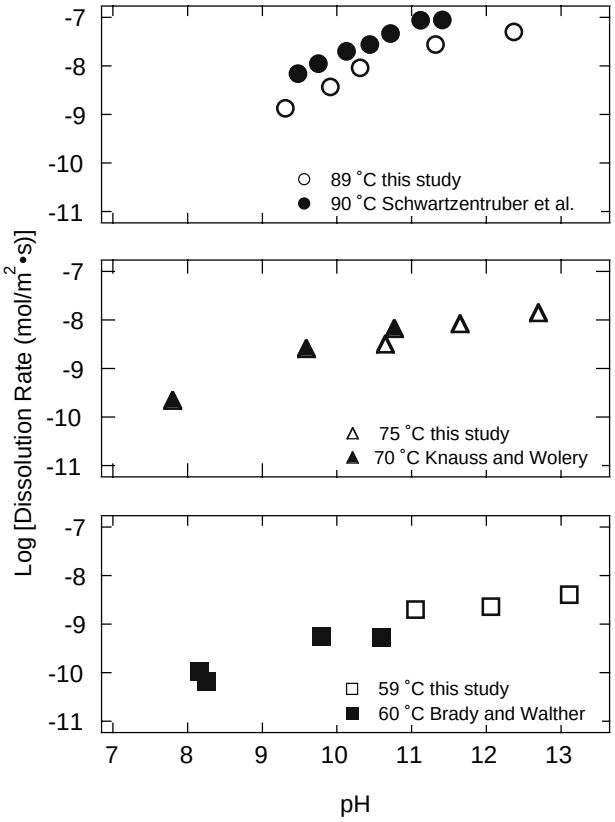

Fig. 2. Baseline (no Al) quartz dissolution rates measured in this study at 59, 75, and 89 °C (open symbols) plotted with rates found in the literature for similar pH and temperature (60, 70, and 90 °C) conditions (filled symbols).

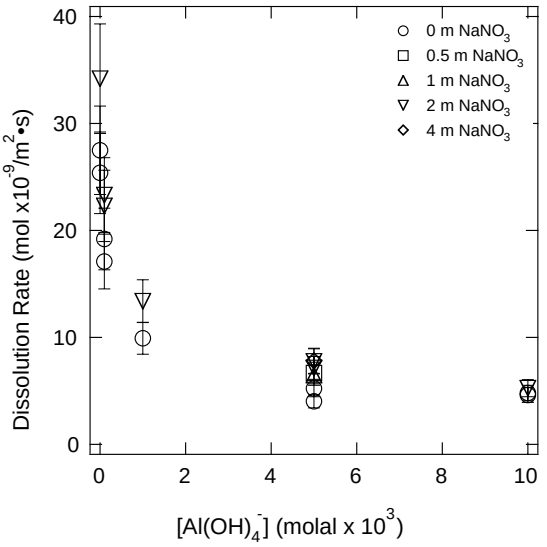

Fig. 3. Quartz dissolution rates at 89 °C, pH 11.3, and various $NaNO_3$ and $Al(OH)_4^-$ concentrations.

approaches a maximum value for each temperature and in situ pH, which depends on the solution conditions.

The effect of temperature on the degree of rate depression appears to be minor, and rate depression can be modeled fairly accurately using the in situ pH and concentration of

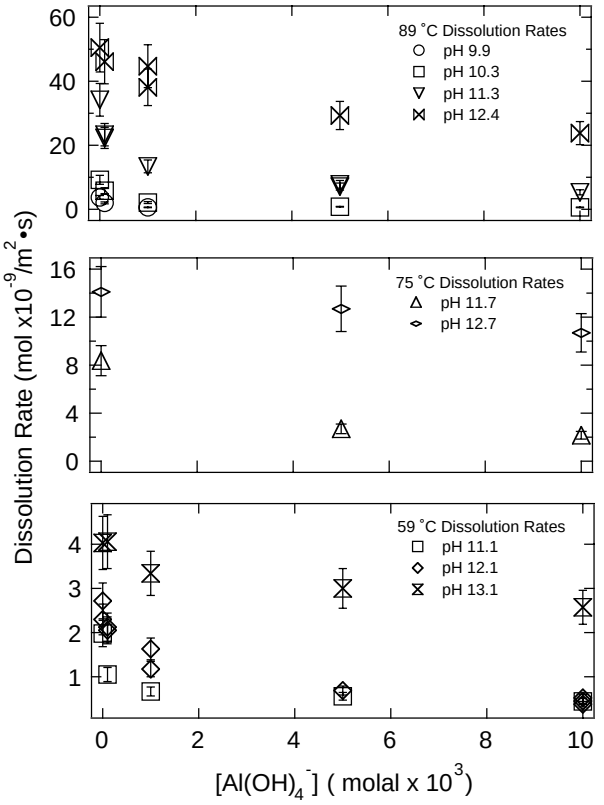

Fig. 4. Quartz dissolution rates at various pH values in 2 m $NaNO_3$ solutions plotted as a function of $[Al(OH)_4^-]$ at 59, 75, and 89 °C. At a given pH, the rate is depressed with increasing $[Al(OH)_4^-]$, until a minimum rate is reached.

$Al(OH)_4^-$. (A mathematical expression and physical interpretation for the rate depression are presented in Section 4) For each $Al(OH)_4^-$ concentration there is an increasing degree of rate depression with decreasing in situ pH, even though each data set at a given $Al(OH)_4^-$ concentration includes dissolution rates at all three temperatures investigated (Fig. 5).

4. Discussion

4.1. Rate depression by $Al(OH)_4^-$

The idea that sorbed Al reduces quartz dissolution rates in alkaline solutions has significant support in the literature, but our results extend those of previous studies and narrow possible interpretations of the phenomenon at high pH. Adsorbed Al species have been shown qualitatively to depress silica dissolution rates in mildly alkaline solutions (Liefländer and Stöber, 1960; Lewin, 1961; Ballou et al., 1973; Iler, 1973; Van Bennekom et al., 1991; Van Cappellen and Qiu, 1997a,b; cf. Jones and Handreck, 1963; Hingston and Raupach, 1967), but the effect at concentrations below saturation with respect to Al-oxyhydroxides is questionable (Dove, 1995). In highly alkaline solutions, Al depresses silica dissolution to a greater extent, although in most of these studies, the saturation

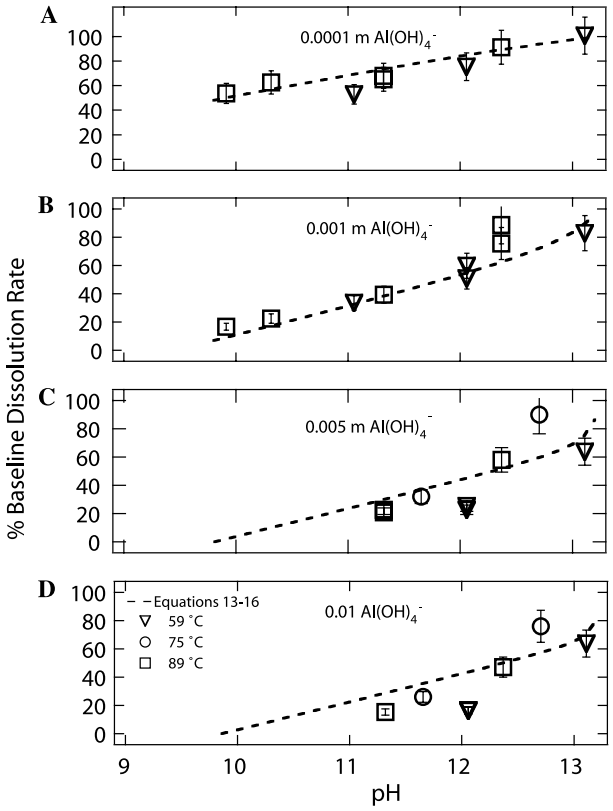

Fig. 5. Quartz dissolution rates in 2 m $NaNO_3$ solutions at temperatures of 59, 75, and 89 °C and (A) 0.0001, (B) 0.001, (C) 0.005, and (D) 0.01 m $Al(OH)_4^-$ concentrations, plotted as a percentage of the baseline rate vs. in situ pH. Lines were calculated using a Langmuir adsorption model described in the Section 4.4.

states of Al-oxyhydroxides were not considered. For example, Sasaki (1962) observed that Al had an inhibiting effect on fused silica dissolution in 0.1 N NaOH at 95 °C (pH ~ 11.3) proportional to log $1/C_{Al}$ (where C_{Al} is the concentration of Al in solution), with complete inhibition occurring at 3.4×10^{-2} N Al. Diallo et al. (1987) showed that the dissolution rate of quartz was reduced by about a factor of 4 in the presence of 7.8×10^{-4}–1.8×10^{-3} M Al in 0.1 N NaOH or KOH (pH ~ 11.8) at 70 °C. Hudson and Bacon (1958) demonstrated that 0.002–0.01 m Al inhibited soda-lime glass (~70% SiO_2) dissolution by 18–53% in 3% NaOH (0.75 N or pH ~ 11.8) at 125 °C. Finally, Labrid and Duquerroix (1991) observed that 4.7×10^{-4} to 2.1×10^{-3} M Al at 30 °C and pH 11.5 inhibited quartz sand dissolution rates by up to a factor of 8 and confirmed that these Al concentrations were below saturation for gibbsite.

Our data also show that dissolved Al inhibits quartz dissolution in alkaline solutions when concentrations are below saturation with respect to Al-oxyhydroxides. However, we have extended the previous results by determining how Al concentration, pH, and temperature in combination affect the rates. Although there are still some points to be resolved, the present results can be used to infer aspects of the nature of the inhibition effect.

The inhibition of dissolution is almost certainly related to the adsorption of $Al(OH)_4^-$ to silanol sites on silica surfaces. For example, Labrid and Duquerroix (1991) estimated that at 30 °C, 2.1×10^{-3} M Al, and pH 11.5, approximately 4 $Al(OH)_4^-$ per nm^2 sorbed on their quartz sand, a sorption site density comparable to that for the density of silanol sites on quartz. In the systems investigated here, silanol groups would exist as >SiOH, $>SiO^-$, and $>SiO^-$–Na^+, and possible adsorption mechanisms might include the following reactions:

$$>\mathrm{SiOH} + \mathrm{Al(OH)_4^-} \Longleftrightarrow >\mathrm{SiOAl(OH)_3^-} + \mathrm{H_2O} \quad (2)$$

$$>\mathrm{SiOH} + \mathrm{Al(OH)_4^-} + \mathrm{Na^+} \Longleftrightarrow >\mathrm{SiOAl(OH)_3^-}\text{–}\mathrm{Na^+} + \mathrm{H_2O} \quad (3)$$

$$>\mathrm{SiO^-} + \mathrm{Al(OH)_4^-} \Longleftrightarrow >\mathrm{SiOAl(OH)_3^-} + \mathrm{OH^-} \quad (4)$$

$$>\mathrm{SiO^-}\text{–}\mathrm{Na^+} + \mathrm{Al(OH)_4^-} \Longleftrightarrow >\mathrm{SiOAl(OH)_3^-}\text{–}\mathrm{Na^+} + \mathrm{OH^-} \quad (5)$$

where > denotes a surface functional group and – denotes outer-sphere complexation.

Labrid and Duquerroix (1991) suggested that $Al(OH)_4^-$ would co-adsorb with Na^+ (Eqs. (3) and (5)), and we can support the idea that the reactions in Eqs. (3) and (5) are dominant by several analogies. First, in solutions with reasonably high Na^+ concentrations, the majority of deprotonated silanol groups are associated with Na^+ sorbed in the outer-sphere plane (e.g., Berger et al., 1994; Dove, 1994; Dove and Elston, 1992; Kent et al., 1988). Leaving Na^+ out of the adsorption reactions (Eqs. (2) and (4)) would result in negatively charged surface sites, which are unlikely to persist to any large extent in a solution with a high Na^+ concentration. Second, several workers (McCormick et al., 1989b; Harris et al., 1997; North and Swaddle, 2000) have used NMR spectroscopy to demonstrate the presence of aluminosilicate species in alkaline solutions, and McCormick et al. (1989b) showed that chemical shifts occurred in ^{23}Na NMR peaks for alkaline solutions when silicate or aluminate species were added. Furthermore, McCormick et al. (1989a) used alkali cation NMR spectroscopy to show that pairing between alkali cations and silicate anions varies with cation size. They inferred that ion pairing between Na^+ and the anionic Si and Al species should enhance the formation of aluminosilicate species, just as it is proposed here that ion pairing of $Al(OH)_4^-$ with Na^+ likely enhances sorption of the aluminate anion onto the negatively charged quartz surface. Finally, Milliken (1950) observed that when aluminosilicate hydrogels were precipitated at pH 9 with low Al content, washed, exchanged with NaCl, and dried, Na^+ was retained in a 1:1 ratio to Al. This Na^+ was readily exchangeable with other cations, which is consistent with the hypothesis that Na^+ facilitates aluminosilicate coagulation by outer-sphere sorption. We suggest a similar mechanism for aluminate adsorption on silica surfaces.

The reactions in Eqs. (3) and (5) indicate that greater Na^+ concentrations in solution should enhance $Al(OH)_4^-$ adsorption. However, this effect is not seen in our data; and, Dove (1994) noted that Na^+ does not appreciably influence silica surface speciation at concentrations above 0.05 m. Since all of our solutions had Na^+ concentrations similar to or larger than 0.05 m (Table A1), it is reasonable to assume that variations in Na^+ concentration would not play much of a role in the sorption reactions represented by Eqs. (3) and (5).

Eqs. (3) and (5) have distinguishing features that may be useful for determining which is dominant. The reaction in Eq. (5) suggests that there should be a temperature dependence at a given in situ pH. As temperature rises from 59 to 89 °C the dissociation constant of water increases by about 0.6 log units from 59 to 89 °C, and consequently the OH^- activity increases by a factor of 4. A higher OH^- activity would decrease $Al(OH)_4^-$ sorption and result in a faster dissolution rate for quartz. Yet, the data in Fig. 5 indicate that if there is such a temperature dependence, it is weak and within experimental error.

On the other hand, the reaction in Eq. (3) would be consistent with the data in Fig. 5 only if several assumptions are made. First, it must be assumed that quartz dissolution rates are proportional to the speciation of silanol groups on the quartz surface. Second, the speciation of the silanol groups must be invariant with temperature for a given in situ pH, i.e., silanol protonation must have an enthalpy of reaction close to zero. Third, the degree of depression of the quartz dissolution rate must be proportional to the amount of aluminate adsorption on the quartz surface. Finally, aluminate adsorption must have an enthalpy of reaction close to zero. Below, we present arguments for the dominance of the reaction in Eq. (3) as well as further discussion on the likely lesser importance of Eq. (5).

4.2. Quartz surface speciation and dissolution in alkaline solutions

Several workers have noted that, at least at 25 °C, silica dissolution rates can be modeled as being approximately proportional to the fraction of deprotonated silanol groups (>SiO^- and >SiO^-– Na^+) on the solid surface (Brady and Walther, 1990; Dove, 1994; Fleming, 1986; House and Orr, 1992; Wirth and Gieskes, 1979), although Guy and Schott (1989) determined an approximately fourth-order dependence. (In this discussion, we assume that the surface complexation behavior of amorphous silica and quartz is equivalent, e.g., see Jørgensen and Jensen, 1967). Dove (1994) compiled published quartz dissolution rate data in NaCl solutions with new hydrothermal rate data and proposed a general equation for quartz dissolution kinetics from 25 to 300 °C and pH 2–13, which includes an approximate first-order dependence on the fraction of deprotonated silanol groups.

Dove (1994) also showed that quartz dissolution rates are enhanced by adsorption of alkali cations, and this enhancement is proportional in magnitude to the hydration energy of the individual alkali cations. Similarly, Berger et al. (1994) and Dove (1999) showed silica dissolution rate enhancement due to the adsorption of Mg^{2+}, Ca^{2+}, and Ba^{2+}, as well as Pb^{2+}, which sorbs in an inner-sphere complex (cf. Karlsson et al., 2001).

Dove (1994) calculated quartz surface speciation using a TLM (Table 2). Initially, this TLM seemed well suited for describing our data because the observed lack of temperature dependence to the rate depression in the presence of $Al(OH)_4^-$ confirms one of the model's important assumptions. Although the surface equilibrium constants in Dove's (1994) TLM (cf., Dove and Elston, 1992) were fit to 25 °C potentiometric titration data, surface speciation was assumed to be invariant with temperature, for a specific in situ pH and Na^+ activity. This assumption is supported by the data of Brady (1992), who showed that silica surface speciation in Na^+ bearing solutions varies only slightly between 25 and 60 °C. (Note that although Brady's (1992) charging curves were virtually indistinguishable below pH 9, they diverged by as much as a factor of 2 above this value. This may be related to the lack of correction for dissolved silica on the basis that it was not significant at 25 °C, but which was not verified for the 60 °C data.) Casey (1994) measured reaction enthalpies for the deprotonation of silanol sites on silica that were significantly smaller (0–10 kJ/mol for a surface with zero net charge) than those

Table 2
Summary of the TLM used by Dove (1994) to predict the speciation of quartz surfaces in NaCl solutions

Reaction	Log K	Source
Surface equilibria		
$>SiOH \Longleftrightarrow\ >SiO^- + H^+$	−6.8	Schindler and Kamber (1968)
$>SiOH + Na^+ \Longleftrightarrow\ >SiO^-\text{–}Na^+ + H^+$	−7.1	Kent et al. (1988)
$>SiOH + H^+ \Longleftrightarrow\ >SiOH_2^+$	2.3	Schindler and Stumm (1987)
$>SiOH + H^+ + Cl^- \Longleftrightarrow\ >SiOH_2Cl$	−6.4	Kent et al. (1988)
Parameter	**Value**	**Source**
Other TLM parameters		
C_1 (o-plane capacitance)	1.25 F/m^2	Kent et al. (1988)
C_2 (β-plane capacitance)	0.2 F/m^2	Kent et al. (1988)
N_s (site density)	4.5 sites/nm^2	Kent et al. (1988)

measured for hydroxyl groups on other oxides (15–30 kJ/mol), which also supports little temperature dependence to surface speciation.

Dove's (1994) extension of the assumption of no temperature dependence for proton adsorption on quartz up to 300 °C may or may not be valid. However, our data combined with those of Brady (1992) are consistent with the hypothesis that the temperature effect is small for the silica surface from 25 to 89 °C. Even if the speciation of silanol groups on quartz surfaces does not change with temperature, the site density might. For instance, Kondo et al. (1992) showed that the site density of silanol groups on colloidal silica changes drastically when subjected to hydrothermal treatment at high pH, probably due to polymerization of deprotonated silanols to form siloxane groups.

To this point, we have argued that quartz dissolution is proportional to surface charging, and that the enthalpy of proton adsorption on quartz surfaces is low. Therefore, surface speciation in the absence of strongly adsorbing ions ought to be essentially invariant with temperature. Furthermore, the dissolution rate depression is probably proportional to the amount of adsorbed $Al(OH)_4^-$, since Figs. 3–5 show that the magnitude of the effect is proportional to the concentration of dissolved $Al(OH)_4^-$. Because there seems to be little effect of temperature on the rate depression, the enthalpy of $Al(OH)_4^-$ adsorption on silanol groups must be near zero. This can be supported by a more detailed argument, based on analogous chemical systems. Although some specific ion adsorption reactions on oxide surfaces have significant enthalpies, others do not (Brady, 1992; Kosmulski, 1994; Kosmulski, 2001). For example, specific Ca^{2+} adsorption on a positively charged alumina surface (analogous to $Al(OH)_4^-$ sorption on a negatively charged quartz surface) is essentially invariant with temperature, given the same surface charge density (Kosmulski, 1994). Kosmulski (1997, 1999) showed that the enthalpy of adsorption for cations of higher valence tends to be more pronounced, and Kosmulski (1996) noted that co-adsorption of Cl^- with Cd^{2+} on alumina reduced the enthalpy of adsorption. This suggests that co-adsorption of $Al(OH)_4^-$ and Na^+ on silanol groups (see Eq. (2)) may have a small enthalpy value.

4.3. Quartz dissolution mechanisms in alkaline solutions

The rate-limiting step in quartz dissolution in aqueous solutions is thought to be the breaking of Si–O bonds in surface siloxane (>Si_2O) groups. Such a mechanism would proceed via nucleophilic attack of H_2O or OH^- on the siloxane bridging bonds. Dove (1994) described two possible siloxane attack mechanisms at quartz surfaces, both of which would depend on surface speciation. First, water molecules could attack surface siloxane groups (>Si_2O) next to neutral silanol groups (>SiOH), creating two new neutral silanol groups.

$$> Si_2O + > SiOH + H_2O \Rightarrow 3 > SiOH \quad (6)$$

Assuming the number of siloxane groups on the surface is approximately constant, the rate of this reaction would be proportional only to the number of neutral silanol sites present. Since the number of neutral silanol groups decreases with increasing pH, this mechanism would become less important in more alkaline solutions. Second, water could attack siloxane groups next to negatively charged silanol groups (>SiO^- or >SiO^-–Me^+, where Me^+ denotes a metal cation sorbed in the outer-sphere plane).

$$> Si_2O + > SiO^- + H_2O \Rightarrow 2 > SiOH + > SiO^- \quad (7)$$

$$> Si_2O + > SiO^-\text{–}Me^+ + H_2O \Rightarrow 2 > SiOH + > SiO^-\text{–}Me^+ \quad (8)$$

Here the reaction rate would be proportional only to the number of negatively charged silanol groups, which becomes larger in more alkaline solutions. Using these two mechanisms, Dove (1994) constructed a generalized rate equation for quartz dissolution from pH 2 to 12, 0–0.3 molal Na^+, and 25–300 °C:

$$R_B = e^{-10.7} T e^{-66000/RT} (\theta_{>SiOH})^1 + e^{4.7} T e^{-82700/RT} (\theta_{>SiO^-_{tot}})^{1.1}, \quad (9)$$

where R_B is the dissolution rate (mol m^{-2} s^{-1}), T is the temperature (Kelvin), R is the gas constant, $\theta_{>SiOH}$ represents the fraction of total surface silanol groups in the neutral form (>SiOH), and $\theta_{>SiO^-_{tot}}$ denotes the fraction of silanol groups in the deprotonated form (>SiO^- or >SiO^-–Na^+). The surface site distributions in Eq. (9) were calculated using the TLM summarized in Table 2. All other parameters in Eq. (9) were determined by least-squares fitting to 271 independent rate measurements from published studies.

Dove (1994) reasoned that since the fitted rate order in Eq. (9) for the >SiOH-catalyzed mechanism is 1 and the rate order for the >SiO^--catalyzed mechanism is close to 1, the reactions in Eqs. (6)–(8) adequately represent the dominant rate-limiting elementary steps in the quartz dissolution process. However, some inconsistencies in the surface speciation calculations used to derive Eq. (9) raise questions about the derived reaction order with respect to >SiO^-.

First, the TLM used was not fit to self-consistent sets of titration data, but was constructed from different surface complexation models in the literature (Table 2). The equilibrium constants for the protonation and deprotonation reactions were taken from constant capacitance models and cannot be transferred to a TLM (Schindler and Stumm, 1987). The equilibrium expressions for the adsorption of Na^+ and the co-adsorption of H^+ and Cl^- were supposedly taken from a TLM constructed by Kent et al. (1988), but in fact, these authors did not report any equilibrium constant for a co-adsorption reaction with H^+ and Cl^-. Rather, they reported equilibrium constants for the Na^+ adsorption and silanol deprotonation reactions. Table 3 summarizes the TLM described by Kent et al. (1988),

which they fit to the potentiometric titration data for Ludox silica reported by Bolt (1957).

Second, when the TLM as described by Dove (1994) was implemented in HYDRAQL and FITEQL, the surface species distributions reported in the appendix of that paper were not reproduced. It is not clear why this discrepancy exists. However, Fig. 6 illustrates the problem by comparing Bolt's (1957) surface charge data for silica in 0.1 M NaCl, the corresponding charging curves predicted by the TLMs of Kent (1988) and Dove (1994) (Tables 1 and 2) and the charging curve reported in Appendix 1 of Dove (1994). Whereas the predictions of the two TLMs accurately fit the titration data (even though Dove's TLM was not consistently formulated), the charging curve reported by Dove (1994) does not. The tabulated surface speciation values in her Appendix 1 were those used in fitting Eq. (9).

What consequences does this discrepancy have for the mechanistic interpretation of quartz dissolution expressed by Eq. (9)? We have taken the quartz dissolution rate data collected by Dove (1994) for alkaline, Na^+-bearing solutions and separated out individual datasets of four or more points for analysis (Bennett et al., 1988; Brady and Walther, 1990; Dove, 1994; House and Orr, 1992; Knauss and Wolery, 1988; Schwartzentruber et al., 1987). The solution conditions and dissolution rate for each experiment, along with the fractions of quartz surface sites in the neutral (>SiOH) and deprotonated ($>SiO^-_{tot}$) forms, as calculated by the TLM of Kent et al. (1988) (see Table 3) are reported in Table B1. If Eq. (9) is correct, then calculated dissolution rates using the recalculated surface speciation values should equal the measured rates. In the log–log plot shown in Fig. 7A, it can be seen that although the data points fall around the 1:1 line, the slopes of the individual data sets cross the line at a fairly consistent angle. Therefore, we adjusted the numerical values in the second half of Eq. (9), associated with the dissolution mechanism

Table 3
Summary of the TLM fit by Kent et al. (1994) to Bolt's (1957) acid–base titration data for Ludox silica surfaces in NaCl solutions

Reaction	Log K
Surface equilibria	
$>SiOH \Longleftrightarrow >SiO^- + H^+$	−6.4
$>SiOH + Na^+ \Longleftrightarrow >SiO^-–Na^+ + H^+$	−7.1
Parameter	**Value**
Other TLM parameters	
C_1 (o-plane capacitance)	1.25 F/m^2
C_2 (β-plane capacitance)	0.2 F/m^2
N_s (site density)	4.5 sites/nm^2

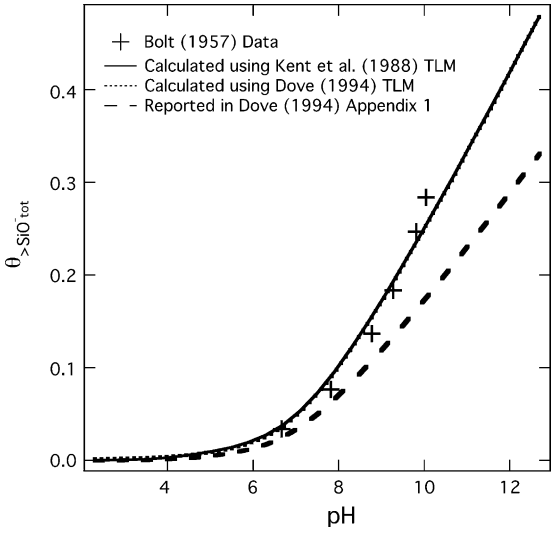

Fig. 6. Fraction of deprotonated sites on a silica surface as measured by Bolt (1957) (symbols), as predicted by triple-layer models described by Kent et al. (1988) and Dove (1994), and as reported by Dove (1994).

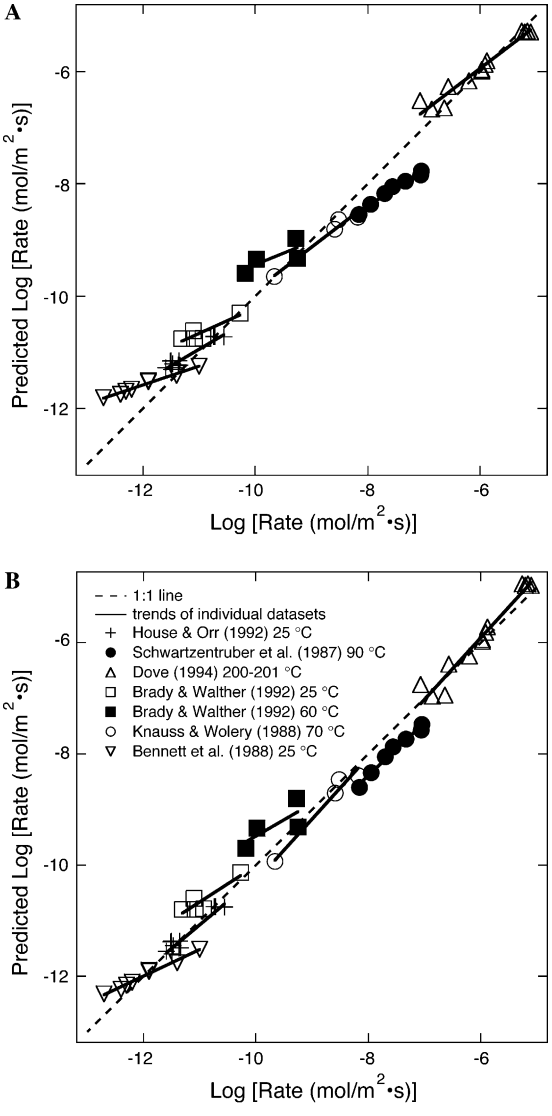

Fig. 7. Predicted vs. measured log dissolution rates of quartz in alkaline solutions. Data points from separate data sets (see Table B1) are represented by different symbols. Predictions were made using (A) Eq. (9) and (B) Eq. (10). The solid lines represent regression lines for the individual data sets. The dashed line represents a 1:1 comparison.

described in Eqs. (7) and (8), by least-squares fitting to the data in Fig. 7A. The new rate equation is expressed as

$$R_B = e^{-10.7} T e^{-66000/RT} (\theta_{>SiOH})^1 + e^{8.0} T e^{-89200/RT} (\theta_{>SiO^-_{tot}})^{1.6}. \quad (10)$$

The new rate order with respect to $\theta_{>SiO^-_{tot}}$ is 1.6, rather than 1.1. Using Eq. (10), the slopes of the individual data sets match the 1:1 line much more closely (Fig. 7B), especially those of the higher temperature data sets, which are expected to be more reliable (Tester et al., 1994). The low T data sets that deviate significantly in slope from the 1:1 line include the 25 °C and 60 °C sets of Brady and Walther (1990), which have poorly constrained slopes with respect to pH, and the 25 °C set of Bennett et al. (1988), which were all carried out at pH 7, with various Na^+ concentrations. Even a small error in the fitted TLM parameters summarized in Table 3 might cause the deviation seen in the latter data set. Rate orders with respect to $\theta_{>SiO^-_{tot}}$ for individual data sets ranged from 1.4 to 3.3 (Table 4).

It may be that the surface speciation calculations we used are responsible for the apparent deviation from first-order behavior. While our speciation calculations are based on a TLM that was fit to experimental data (see Fig. 6), those data did not extend to some of the extreme pH values represented in Tables 3 and B1. Furthermore, it is possible that a single type of negatively charged site is insufficient to describe quartz surfaces, a fact that would become more apparent at extreme pH values (Bickmore et al., 2004). However, if the speciation calculations are approximately correct, there is clearly another dissolution mechanism operating in alkaline solutions. The hypothesis that another mechanism is operative might explain why some of the data sets in Fig. 7B are not fit as well as others by Eq. (10).

In particular, we are able to demonstrate that our quartz dissolution rates cannot be proportional to surface charge density, assuming this value does not change much over 25–89 °C. The surface charge density for the data point with the lowest pH in each of our 2 m $NaNO_3$ data sets (59, 75, and 89 °C) was estimated by interpolating between Bolt's (1957) titration data for 1 and 4 M NaCl (Fig. 8). The surface charge density for each subsequent point in the data sets was estimated by assuming that the dissolution rate is proportional to $\theta_{>SiO^-_{tot}}$. This procedure predicts

Table 4
Sets of quartz dissolution data containing four or more points in the alkaline pH range extracted from Table 2 of Dove (1994)

Source	Temperature (°C)	pH range	Rate order[a]
House and Orr (1992)	25	8.25–10.49	1.7
Schwartzentruber et al. (1987)	90	9.48–11.41	1.7
Dove (1994)	200–201	6.9–9.1	1.4
Brady and Walther (1990)	25	10.3–12.3	2.6
Brady and Walther (1990)	60	8.16–10.6	1.6
Knauss and Wolery (1988)	70	7.8–10.77	1.4
Bennett et al. (1988)[a]	25	7	3.3

[a] Calculated with respect to $>SiO^-_{tot}$ using surface speciation values obtained from the TLM of Kent et al. (1988) (see Table 3, this paper).

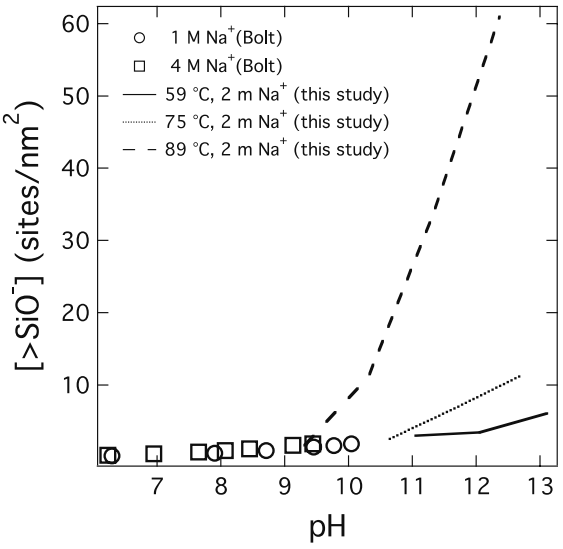

Fig. 8. Symbols represent Bolt's (1957) 1 and 4 M NaCl surface charge data for Ludox silica. Lines represent estimates of quartz surface charge for the pH and Na^+ concentration conditions in our 2 m $NaNO_3$ baseline (no Al) quartz dissolution experiments. The estimates were made by interpolating the lowest-pH point at each temperature between the surface charge curves of Bolt (1957). Subsequent estimates were made by assuming that surface charge is linearly proportional to dissolution rate. However, this assumption does not produce physically reasonable surface charge estimates.

surface charge densities higher than what might be predicted by extrapolation of Bolt's (1957) curves. Even though there may be significant error in Bolt's (1957) data at high pH, the true surface charge would probably be lower than that predicted by titration because the data are not corrected for silica dissolution. Furthermore, at 89 °C, predicted surface charge densities rise to over 60 $>SiO^-_{tot}$ sites/nm^2, which is physically unrealistic (Carroll et al., 2002). The deviation from the measured surface charge trends becomes larger with higher temperature. Published dissolution rates at similar temperatures and pH values would be expected to show similar features (see Fig. 2).

What other dissolution mechanism might be involved? Xiao and Lasaga (1996) used quantum mechanical cluster calculations to show that quartz dissolution could proceed either by the mechanism described by Eqs. (7) and (8) (see Fig. 9A) or by attack of OH^- ions on siloxane groups, catalyzed by the presence of a neutral silanol group (Fig. 9B). This can be described by the following reaction

$$>Si_2O + >SiOH + OH^- \Rightarrow 2>SiOH + >SiO^- \quad (11)$$

Alternatively, electrolyte cations might catalyze this reaction.

$$>Si_2O + >SiOH + Me^+ + OH^- \Rightarrow 2>SiOH + >SiO^- – Me^+ \quad (12)$$

Both mechanisms (i.e., those described in Eqs. (7), (8) and Eqs. (11), (12)) would result in the same activated complex. In the second mechanism (Eqs. (11), (12)), the dissolution rate would be inversely proportional to the fraction of deprotonated surface sites, but proportional to the concentration

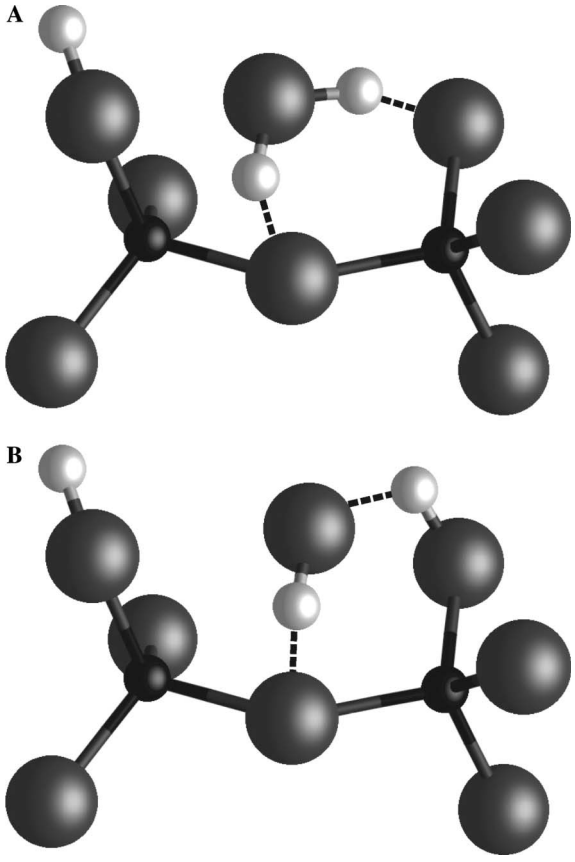

Fig. 9. (A) First step in the quartz dissolution mechanism as proposed by Dove (1994). A water molecule attacks the oxygen atom of a siloxane group and is catalyzed by the presence of a $>SiO^-$ group (see Dove, 1994). (B) First step in an alternate quartz dissolution mechanism as proposed by Xiao and Lasaga (1996). A hydroxide ion attacks the oxygen atom of a siloxane group and is catalyzed by the presence of a >SiOH group.

of OH^-. Since for a given in situ pH the OH^- activity, and hence concentration, would go up with temperature (up to about 250 °C), but the fraction of deprotonated surface sites would remain constant, the second mechanism would tend to dominate at higher pH and higher temperature. This might explain why our high pH dissolution rates deviate more from proportionality with surface charge density at higher temperature, and why a number of studies have shown that silica dissolution rates are approximately proportional to surface charge density at lower temperature and lower pH values. This explanation is also consistent with the fact that the rate order of our baseline dissolution rates as a function of pH increased with temperature. (We have not explicitly calculated these rate orders because we do not trust the TLM used to reliably estimate quartz surface speciation at the high pH values investigated here. However, an increase in rate order with temperature can be inferred by visual inspection of Fig. 8.) Therefore, it seems probable that both dissolution mechanisms (Eqs. (7), (8) and (11), (12)) operate in alkaline solutions.

We have not yet attempted to test this proposition by constructing another generalized rate equation analogous to Eqs. (9) and (10), and fitting it to all available rate data. Further work will address this in a statistically rigorous manner and will necessarily include estimates of both surface speciation and near-surface OH^- concentration. For the purpose of this paper, we merely conclude that the relationship between quartz surface speciation and dissolution rate has yet to be definitively determined.

4.4. Empirical model of effect of $Al(OH)_4^-$ on dissolution rate

If the rates of the siloxane attack mechanisms controlling quartz dissolution depend on the number of surface >SiOH and $>SiO^-$ groups, then we may explain the effect of $Al(OH)_4^-$ in terms of adsorption on, and passivation of, these silanol sites. When a plausible mechanistic interpretation of quartz dissolution in terms of surface speciation is available, it should be extended to include the effect of adsorbed $Al(OH)_4^-$, only if reliable adsorption data are obtained. It is difficult to measure adsorption on quartz at high pH because the surface dissolves rapidly. Therefore, for now, a simple empirical model is presented to describe how quartz dissolution is passivated by the postulated adsorption of $Al(OH)_4^-$.

If it is assumed that siloxane attack is negligibly slow around passivated sites, we can express the dissolution rates according to the following equation:

$$\log R_{Al} = \log R_B + \log(1 - \theta_{Al}). \quad (13)$$

where R_{Al} is the rate, R_B is the baseline (no Al) rate under otherwise identical conditions, and θ_{Al} is the fraction of the quartz surface passivated by $Al(OH)_4^-$ adsorption. A Langmuir isotherm model with the following form, modified from Langmuir (1997), in combination with Eq. (13) was fit to our data

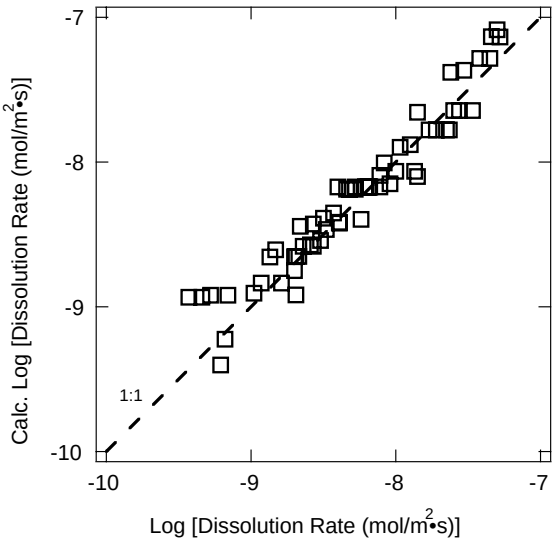

Fig. 10. Comparison of quartz dissolution rates calculated using Eqs. (1) and (13)–(16) with measured rates. The line represents a 1:1 comparison. Compare the measured and predicted log rate values in Table A1 to determine which data points deviate most significantly from the model predictions.

$$\frac{1}{\theta_{Al}} = \frac{1}{bC\theta_{max}} + \frac{1}{\theta_{max}}, \quad (14)$$

where C is the aqueous concentration of $Al(OH)_4^-$, θ_{max} is the maximum fraction of the surface that can be passivated by $Al(OH)_4^-$ adsorption at a given pH, and b is a constant at a given pH. It was assumed that both b and θ_{max} vary linearly with in situ pH, and equations for each were fit to the rate depression data. The following equations were generated:

$$b = -3000pH + 39700. \quad (15)$$

$$\theta_{max} = -0.196pH + 2.94. \quad (16)$$

Using quadratic equations for the variation of these parameters with pH did not improve the fit.

The lines in Fig. 5 were fit to the data using Eqs. (13)–(16). This model reproduces the general features of the data, including greater rate depression at lower pH and higher $Al(OH)_4^-$ concentration, and a leveling off of the rate depression with higher $Al(OH)_4^-$ concentration for a given in situ pH, although the data for lower $Al(OH)_4^-$ concentrations are predicted most accurately. It may be that a Langmuir isotherm does not describe adsorption at high concentrations as well, due to some change in the process such as the formation of a distinct aluminosilicate surface phase.

The rate correction described by Eqs. (13)–(16) was combined with Eq. (1) to predict dissolution rates for all experimental conditions studied (Table A1, Fig. 10). The standard error for the calculated rates was ±0.15 log units.

Appendix A

See Table A1.

5. Summary

We have demonstrated that dissolved Al at concentrations below Al-oxyhydroxide solubility significantly inhibits the dissolution of quartz. Predictive models of the phenomenon have been developed which can easily be incorporated into reactive transport codes. Perhaps more important, we have provided evidence that a standard model of quartz dissolution (Dove, 1994) includes points that need to be adjusted or expanded to accurately predict quartz dissolution rates in a theoretically robust manner under alkaline conditions. Particularly needed are self-consistent studies of the relationship between surface charge density, near-surface OH^- concentration, and quartz dissolution rate that extend to elevated pH and temperature.

Acknowledgments

We thank the US Department of Energy Environmental Management Science Program for support under Grant DE-FG07-99ER15009 to K. Nagy and contract DE-AC06-76RLO 1830 to J. Serne and S. Yabusaki at Pacific Northwest National Laboratory (PNNL), and the donors of the Petroleum Research Fund of the American Chemical Society (Grant #38775-GB5S to B. Bickmore). Carrick Eggleston, Kevin Knauss, Patricia Dove, and one anonymous reviewer offered helpful comments on the manuscript. We also thank P. Sandlin for his contribution to the laboratory work.

Associate editor: Carrick M. Eggleston

Table A1
Solution parameters and quartz dissolution rates for the experiments of this study

Sample ID	Temp. (°C)	pH[a]	$[Na^+]$ (m)	$[NO_3^-]$ (m)	$[Al(OH)_4^-]$ (m)	$[OH^-]$ (m)	log Rate[b]	Predicted log Rate
A0	89	11.3	0.1	0	0	0.1	−7.60	−7.64
A1	89	11.3	0.14	0.03	0.01	0.1	−8.34	−8.19
1A	89	12.3	1	0	0	1	−7.28	−7.14
2A	89	11.3	0.1	0	0	0.1	−7.56	−7.64
3A	89	9.4	0.001	0	0	0.001	−8.83	−8.61
5A	89	12.4	3	2	0	1	−7.30	−7.09
6A	89	11.3	2.1	2	0	0.1	−7.47	−7.64
7A	89	9.3	2.001	2	0	0.001	−8.87	−8.66
8A	89	10.3	2.01	2	0	0.01	−8.04	−8.15
9A	89	10.4	0.01	0	0	0.01	−7.85	−8.10
2B	89	11.3	0.14	0.03	0.01	0.1	−8.32	−8.19
3B	89	11.3	0.104	0.003	0.001	0.1	−8.00	−8.06
5B	89	11.3	2.14	2.03	0.01	0.1	−8.28	−8.19
6B	89	11.3	2.104	2.003	0.001	0.1	−7.87	−8.06
1C	89	11.3	0.12	0.015	0.005	0.1	−8.40	−8.17
2C	89	11.3	2.12	2.015	0.005	0.1	−8.21	−8.17
3C	89	11.3	0.1004	0.0003	0.0001	0.1	−7.77	−7.78
4C	89	11.3	2.1004	2.0003	0.0001	0.1	−7.65	−7.78
5C	89	11.3	0.12	0.015	0.005	0.1	−8.28	−8.17
6C	89	11.3	2.12	2.015	0.005	0.1	−8.11	−8.17
7C	89	11.3	0.1004	0.0003	0.0001	0.1	−7.72	−7.78

(*continued on next page*)

Table A1 (*continued*)

Sample ID	Temp. (°C)	pH[a]	$[Na^+]$ (m)	$[NO_3^-]$ (m)	$[Al(OH)_4^-]$ (m)	$[OH^-]$ (m)	log Rate[b]	Predicted log Rate
8C	89	11.3	2.1004	2.0003	0.0001	0.1	−7.63	−7.78
9C	89	11.3	0.62	0.515	0.005	0.1	−8.18	−8.17
10C	89	11.3	1.12	1.015	0.005	0.1	−8.19	−8.17
11C	89	11.4	4.12	4.015	0.005	0.1	−8.11	−8.09
12C	89	12.4	3.04	2.03	0.01	1	−7.62	−7.38
13C	89	12.4	3.02	2.015	0.005	1	−7.53	−7.37
14C	89	12.4	3.004	2.003	0.001	1	−7.35	−7.28
15C	89	12.4	3.004	2.003	0.001	1	−7.42	−7.28
18C	89	12.4	3.0004	2.0003	0.0001	1	−7.34	−7.13
3D	89	10.3	2.014	2.003	0.001	0.01	−8.69	−8.92
4D	89	10.3	2.0104	2.0003	0.0001	0.01	−8.24	−8.40
1F	59	13.1	3	2	0	1	−8.39	−8.42
2F	59	13.1	3.04	2.03	0.01	1	−8.59	−8.57
3F	59	13.1	3.02	2.015	0.005	1	−8.52	−8.54
4F	59	13.1	3.004	2.003	0.001	1	−8.48	−8.47
5F	59	13.1	3.0004	2.0003	0.0001	1	−8.39	−8.42
6F	59	12.1	2.1	2	0	0.1	−8.57	−8.58
7F	59	12.1	2.14	2.03	0.01	0.1	−9.34	−8.93
8F	59	12.1	2.12	2.015	0.005	0.1	−9.16	−8.92
9F	59	12.1	2.104	2.003	0.001	0.1	−8.79	−8.84
10F	59	12.1	2.1004	2.0003	0.0001	0.1	−8.69	−8.65
11F	59	11.1	2.01	2	0	0.01	−8.70	−8.75
14F	59	11.1	2.014	2.003	0.001	0.01	−9.18	−9.22
15F	59	11.1	2.0104	2.0003	0.0001	0.01	−8.98	−8.91
16F	59	12.1	2.1	2	0	0.1	−8.64	−8.58
17F	59	12.1	2.12	2.015	0.005	0.1	−9.28	−8.92
18F	59	12.1	2.14	2.03	0.01	0.1	−9.43	−8.93
19F	59	12.1	2.104	2.003	0.001	0.1	−8.93	−8.84
20F	59	12.1	2.1004	2.0003	0.0001	0.1	−8.67	−8.65
1E	75	12.7	3	2	0	1	−7.85	−7.66
2E	75	11.7	2.1	2	0	0.1	−8.08	−8.01
3E	75	10.6	2.01	2	0	0.01	−8.50	−8.39
4E	75	12.7	3.04	2.03	0.01	1	−7.97	−7.90
5E	75	12.7	3.02	2.015	0.005	1	−7.90	−7.88
6E	75	11.7	2.14	2.03	0.01	0.1	−8.66	−8.44
7E	75	11.7	2.12	2.015	0.005	0.1	−8.57	−8.43
1G	89	9.9	2.004	2	0	0.004	−8.43	−8.35
2G	89	9.9	2.008	2.003	0.001	0.004	−9.21	−9.40
3G	89	9.9	2.0044	2.0003	0.0001	0.004	−8.70	−8.65

The predicted log rate values refer to Eqs. (8)–(10) and Eqs. (13)–(16)(cf. Fig. 10).

[a] The pH values reported here are calculated at temperature using the Pitzer model described in the text.

[b] Rate in mol/m^2 s.

Appendix B

See Table B1.

Table B1
Published solution parameters and quartz dissolution rate data taken from Table 2 of Dove (1994) for alkaline, Na-bearing solutions, along with quartz surface speciation calculated using the TLM of Kent et al. (1988). Only data sets with four or more points are included

Sample	$[Na^+]$ (m)	pH	T (°C)	$\theta_{>SiOH}$[a]	$\theta_{>SiO^-_{tot}}$[b]	Log Rate[c]
House and Orr (1992)						
H&O*14	0.01	8.25	25	0.939	0.061	−11.49
H&O*15	0.01	8.35	25	0.934	0.066	−11.59
H&O*20	0.01	8.46	25	0.929	0.071	−11.37
H&O*13	0.01	8.47	25	0.928	0.072	−11.34
H&O*12	0.01	8.48	25	0.927	0.073	−11.37
H&O*17	0.01	8.55	25	0.924	0.076	−11.47
H&O*19	0.01	8.7	25	0.915	0.085	−11.51
H&O*16	0.01	8.72	25	0.914	0.086	−11.36
H&O*18	0.01	8.72	25	0.914	0.086	−11.5

Table B1 (*continued*)

Sample	$[Na^+]$ (m)	pH	T (°C)	$\theta_{>SiOH}$[a]	$\theta_{>SiO^-_{tot}}$[b]	Log Rate[c]
H&O*20	0.01	10.46	25	0.793	0.207	−10.56
H&O*20	0.01	10.46	25	0.793	0.207	−10.56
H&O*20	0.01	10.49	25	0.790	0.210	−10.72
H&O*20	0.01	10.49	25	0.790	0.210	−10.74
Schwartzentruber et al. (1987)						
S et al.*1	0.001	9.48	90	0.927	0.073	−8.16
S et al.*2	0.002	9.75	90	0.894	0.106	−7.95
S et al.*3	0.005	10.13	90	0.841	0.159	−7.7
S et al.*4	0.01	10.44	90	0.794	0.206	−7.56
S et al.*5	0.02	10.72	90	0.748	0.252	−7.33
S et al.*6	0.05	11.12	90	0.682	0.318	−7.06
S et al.*7	0.1	11.41	90	0.632	0.368	−7.05
Dove (1994)						
12*34	0.0001	7.04	200	0.991	0.009	−6.86
12*63	0.05	6.93	200	0.963	0.037	−5.97
16*10	0.05	6.93	200	0.963	0.037	−5.97
16*16	0.05	9.1	200	0.843	0.157	−5.1
16*19	0.05	9.1	200	0.843	0.157	−5.21
14*13	0.06	9.1	200	0.837	0.163	−5.16
14*16	0.06	9.1	200	0.837	0.163	−5.26
12*65B	0.0001	7.04	201	0.991	0.009	−6.64
12*68	0.0001	7.56	201	0.988	0.012	−7.07
12*71	0.001	7.6	201	0.980	0.020	−6.57
12*74	0.01	7	201	0.976	0.024	−6.2
12*77	0.05	6.94	201	0.963	0.037	−5.97
12*80	0.1	6.9	201	0.955	0.045	−5.91
12*83	0.15	6.9	201	0.948	0.052	−5.88
Brady and Walther (1990)						
B&W*Q25	0.002	11	25	0.805	0.195	−11.08
B&W*S25	0.002	11.04	25	0.802	0.198	−10.93
B&W*KCl3	0.01	10.3	25	0.805	0.195	−11.31
B&W*6B	0.07	10.27	25	0.740	0.260	−11.1
B&W*Gamm	0.52	12.3	25	0.494	0.506	−10.27
Brady and Walther (1990)						
B&W*S60	0.007	9.79	60	0.855	0.145	−9.25
B&W*Q60	0.027	8.25	60	0.917	0.083	−10.18
B&W*12,3	0.11	10.6	60	0.697	0.303	−9.28
B&W*R60	0.269	8.16	60	0.859	0.141	−9.98
Knauss and Wolery (1988)[d]						
K&W*3	0.004	7.8	70	0.968	0.032	−9.66
K&W*5	0.044	9.59	70	0.810	0.190	−8.59
K&W*6	0.062	10.77	70	0.703	0.297	−8.18
K&W*6	0.104	10.22	70	0.730	0.270	−8.52
Bennett et al. (1988)[e]						
QDL1-G (25)	0.006	7	25	0.979	0.021	−12.7
QDL1-H (25)	0.05	7	25	0.961	0.039	−11.9
QDL1-I (25)	0.1	7	25	0.951	0.049	−11.4
QDL1-J (25)	0.3	7	25	0.930	0.070	−11
QDL2-R (25)	0.01	7	25	0.976	0.024	−12.4
QDL2-S (25)	0.015	7	25	0.973	0.027	−12.3
QDL2-T (25)	0.02	7	25	0.971	0.029	−12.2
QDL2-U (25)	0.055	7	25	0.960	0.040	−11.9

[a] Fraction of surface silanol sites in the >SiOH form.
[b] Fraction of surface silanol sites in the $>SiO^-$ or $>SiO^-$–Na^+ form.
[c] Rate in mol/m^2 s.
[d] Sample K&W*4 was excluded from this data set because it is identical to K&W*3 and should not have been included in Table 2 of Dove (1994) (Kevin Knauss, personal communication).
[e] Sample QDL1-A (25) was excluded from this data set because it was incorrectly labeled as pH 7, rather than pH 5.7, in Table 2 of Dove (1994).

Appendix C. Supplementary data

This annex includes the solution analyses used to obtain quartz dissolution rates via the method of initial rates. Supplementary data associated with this article can be found, in the online version, at doi:10.1016/j.gca.2005.09.017.

References

Azaroual, M., Fouillac, C., Matray, J.M., 1997. Solubility of silica polymorphs in electrolyte solutions, I. Activity coefficient of aqueous silica from25 °C to 250 °C, Pitzer's parameterisation. *Chem. Geol.* **140**, 155–165.

Bagci, S., Kok, M.V., Turskoy, U., 2000. Determination of formation damage in limestone reservoirs and its effect on production. *J. Petrol. Sci. Eng.* **28**, 1–12.

Ballou, E.V., Leban, M.I., Wydeven, T., 1973. Solute rejection by porous glass membranes .III. Reduced silica dissolution and prolonged hyperfiltration service with feed additives. *J. Appl. Chem. Biotechnol.* **23**, 119–130.

Bates, R.G., 1964. *Determination of pH*. Wiley, New York.

Bennett, P.C., Melcer, M.E., Siegel, D.I., Hassett, J.P., 1988. The dissolution of quartz in dilute aqueous solutions of organic acids at 25 °C. *Geochim. Cosmochim. Acta* **52**, 1521–1530.

Berger, G., Cadore, E., Schott, J., Dove, P.M., 1994. Dissolution rate of quartz in lead and sodium electrolyte solutions between 25 and 300 °C: Effect of the nature of surface complexes and reaction affinity. *Geochim. Cosmochim. Acta* **58**, 541–551.

Bethke, C.M. (1998) The Geochemist's Workbench, Release 3.0, University of Illinois at Urbana-Champaign.

Bickmore, B.R., Nagy, K.L., Young, J.S., Drexler, J.W., 2001. Nitrate–cancrinite precipitation on quartz sand in simulated Hanford tank solutions. *Environ. Sci. Technol.* **35**, 4481–4486.

Bickmore, B.R., Tadanier, C.J., Rosso, K.M., Monn, W.D., Eggett, D.L., 2004. Bond-Valence methods for pK_a prediction: critical reanalysis and a new approach. *Geochim. Cosmochim. Acta* **68**, 2025–2042.

Bolt, G.H., 1957. Determination of the charge density of silica sols. *J. Phys. Chem.* **61**, 1166–1169.

Brady, P.V., 1992. Silica surface chemistry at elevated temperatures. *Geochim. Cosmochim. Acta* **56**, 2941–2946.

Brady, P.V., Walther, J.V., 1990. Kinetics of quartz dissolution at low temperatures. *Chem. Geol.* **82**, 253–264.

Busey, R.H., Mesmer, R.E., 1977. Ionization equilibria of silicic acid and polysilicate formation in aqueous sodium chloride solutions to 300 °C. *Inorgan. Chem.* **16**, 2444–2450.

Carroll, S.A., Maxwell, R.S., Bourcier, W., Martin, S., Hulsey, S., 2002. Evaluation of silica–water surface chemistry using NMR spectroscopy. *Geochim. Cosmochim. Acta* **66**, 913–926.

Casey, W.H., 1994. Enthalpy changes for Bronsted acid–base reactions on silica. *J. Colloid Interface Sci.* **163**, 407–419.

Catalano, J.G., Heald, S.M., Zachara, J.M., Brown, G.E., 2004. Spectroscopic and diffraction study of uranium speciation in contaminated vadose zone sediments from the Hanford Site, Washington State. *Environ. Sci. Technol.* **38**, 2822–2828.

Cherrey, K.D., Flury, M., Harsh, J.B., 2003. Nitrate and colloid transport through coarse Hanford sediments under steady state, variably saturated flow. *Water Resour. Res.* **39**, 1165.

Chorover, J., Choi, S.K., Amistadi, M.K., Karthikeyan, K.G., Crosson, G., Mueller, K.T., 2003. Linking cesium and strontium uptake to kaolinite weathering in simulated tank waste leachate. *Environ. Sci. Technol.* **37**, 2200–2208.

Chou, L., Wollast, R., 1985. Steady-state kinetics and dissolution mechanisms of albite. *Am. J. Sci.* **285**, 963–993.

Diallo, M.S., Jenkins-Smith, N.L., Bunge, A.L., 1987. Dissolution rates for quartz, aluminum bearing minerals, and their mixtures in sodium and potassium hydroxide, SPE paper16276. International Symposium on Oilfield Chemistry, San Antonio, Texas, Feb. 4–6, 1987, 359–368.

Dougan, W.K., Wilson, A.L., 1974. The absorptiometric determination of aluminium in water. A comparison of some chromogenic reagents and the development of an improved method. *Analyst* **99**, 413–430.

Dove, P.M., 1994. The dissolution kinetics of quartz in sodium chloride solutions at 25–300 °C. *Am. J. Sci.* **294**, 665–712.

Dove, P.M., 1995. Kinetic and thermodynamic controls on silica reactivity in weathering environments. In: White, A.F., Brantley, S.L. (Eds.), *Chemical Weathering Rates of Silicate Minerals,*, *Reviews in Mineralogy*, Vol. 31. Mineralogical Society of America, Washington, DC, pp. 235–290.

Dove, P.M., 1999. The dissolution kinetics of quartz in aqueous mixed cation solutions. *Geochim. Cosmochim. Acta* **63**, 3715–3727.

Dove, P.M., Elston, S.F., 1992. Dissolution kinetics of quartz in sodium chloride solutions: analysis of existing data and a rate model for 25 °C. *Geochim. Cosmochim. Acta* **56**, 4147–4156.

Drever, J.I., 1997. *The Geochemistry of Natural Waters: Surface and Groundwater Environments*, 3rd ed. Prentice-Hall, Upper Saddle River, NJ.

Fleming, B.A., 1986. Kinetics of reaction between silicic acid and amorphous silica surfaces in NaCl solutions. *J. Colloid Interface Sci.* **110**, 40–64.

Flury, M., Mathison, J.B., Harsh, J.B., 2002. In situ mobilization of colloids and transport of cesium in Hanford sediments. *Environ. Sci. Technol.* **36**, 5335–5341.

Gephart, R.E., Lundgren, R.E., 1998. *Hanford Tank Cleanup*. Battelle, Columbus.

Guy, C., Schott, J., 1989. Multisite surface reaction versus transport control during the hydrolysis of a complex oxide. *Chem. Geol.* **78**, 181–204.

Harris, R.K., Samadi-Maybodi, A., Smith, W., 1997. *Zeolites* **19**, 147–155.

He, Y.T., Bigham, J.M., Traina, S.J., 2005. Biotite dissolution and Cr(VI) reduction at elevated pH and ionic strength. *Geochem. Cosmochim. Acta* **69**, 3791–3800.

Hershey, J.P., Millero, F.J., 1986. The dependence of the acidity constants of silicic acid on NaCl concentration using Pitzer's equations. *Mar. Chem.* **18**, 101–105.

Hingston, F.J., Raupach, M., 1967. The reaction between monosilicic acid and aluminium hydroxide. I. Kinetics of adsorption of silicic acid by aluminium hydroxide. *Austr. J. Soil Res.* **5**, 295–309.

Hoch, A.R., Linklater, C.M., Noy, D.J., Rodwell, W.R., 2004. Modelling the interaction of hyperalkaline fluids with simplified rock mineral assemblages. *Appl. Geochem.* **19**, 1431–1451.

Hornof, V., Neale, G.H., Gholam-Hosseini, M., 2000. Effects of flow rate and alkali-to-acid ratio on the displacement of acidic oil by alkaline solutions in radial porous media. *J. Colloid Interface Sci.* **231**, 196–198.

House, W.A., 1994. The role of surface complexation in the dissolution kinetics of silica: effects of monovalent and divalent ions at 25 °C. *J. Colloid Interface Sci.* **163**, 379–390.

House, W.A., Orr, D.R., 1992. Investigation of the pH dependence of the kinetics of quartz dissolution at 25 °C. *J. Chem. Soc. Faraday Trans.* **88**, 233–241.

Hudson, G.A., Bacon, F.R., 1958. Inhibition of alkaline attack on soda-lime glass. *Ceramic Bull.* **37**, 185–188.

Iler, R.K., 1973. Effect of adsorbed alumina on the solubility of amorphous silica in water. *J. Colloid Interface Sci.* **43**, 399–408.

Jones, L.H.P., Handreck, K.A., 1963. Effects of iron and aluminium oxides on silica in solution in soils. *Nature* **198**, 852–853.

Jørgensen, S.S., Jensen, A.T., 1967. Acid–base properties of quartz suspensions. *J. Phys. Chem.* **71**, 745–750.

Karlsson, M., Craven, C., Dove, P.M., Casey, W.H., 2001. Surface charge concentrations on silica in different 1.0 M metal-chloride background electrolytes and implications for dissolution rates. *Aquat. Geochem.* **7**, 13–32.

Kent, D.B., Tripathi, V.S., Ball, N.B., Leckie, J.O., Siegel, M.D., 1988. Surface-complexation modeling of radionuclide adsorption in subsurface environments. Albuquerque, New Mexico, Sandia National Laboratories, U.S. Nuclear Regulatory Commission Report NUREG/CR-4807, 113 pp.

Knauss, K., Wolery, T., 1988. The dissolution kinetics of quartz as a function of pH and time at 70 °C. *Geochim. Cosmochim. Acta* **52**, 43–53.

Kondo, S., Igariashi, M., Nakai, K., 1992. The properties of silica surfaces treated at high pH. *Colloids Surf.* **63**, 33–37.

Koroleff, F., 1983. Determination of silicon. In: Grasshoff, K., Ehrhardt, M., Kremling, K. (Eds.), *Methods of Seawater Analysis*, 2nd Ed. Verlag Chemie, New York, pp. 174–183.

Kosmulski, M., 1994. Co-adsorption of mono- and multivalent ions on silica and alumina. *Berichte der Bunsen-Gesellschaft für Physikalische Chemie* **98**, 1062–1067.

Kosmulski, M., 1996. Adsorption of cadmium on alumina and silica: Analysis of the values of stability constants of surface complexes calculated for different parameters of triple layer model. *Colloids Surf. A* **117**, 201–214.

Kosmulski, M., 1997. Standard enthalpies of adsorption of di- and trivalent cations on alumina. *J. Colloid Interface Sci.* **192**, 215–227.

Kosmulski, M., 1999. Adsorption of trivalent cations on silica. II. Temperature effect. *J. Colloid Interface Sci.* **211**, 410–412.

Kosmulski, M., 2001. *Chemical Properties of Material Surfaces*. Marcel Dekker, New York.

Labrid, J., Duquerroix, J.P., 1991. Thermodynamic and kinetic aspects of the dissolution of quartz–kaolinite mixtures by alkalis. *Revue de L'Institut Francais du Pétrole* **46**, 41–59.

Langmuir, D., 1997. *Aqueous Environmental Geochemistry*. Prentice-Hall, Upper Saddle River, NJ.

Lewin, J.C., 1961. The dissolution of silica from diatom walls. *Geochim. Cosmochim. Acta* **21**, 182–198.

Liefländer, M., Stöber, W., 1960. Topochemische reaktionen von Quarz, amorphem siliciumdioxyd und titandioxyd mit aluminiumtriisobutyl. *Z. Naturforsch. B* **15**, 411–413.

Mashal, K., Harsh, J.B., Flury, M., Felmy, A.R., Zhao, H.T., 2004. Colloid formation in Hanford sediments reacted with simulated tank waste. *Environm. Sci. Technol.* **38**, 5750–5756.

McCormick, A.V., Bell, A.T., Radke, C.J., 1989a. Evidence from alkali-metal NMR spectroscopy for ion-pairing in alkaline silicate solutions. *J. Phys. Chem.* **93**, 1733–1737.

McCormick, A.V., Bell, A.T., Radke, C.J., 1989b. Multinuclear NMR investigation of the formation of aluminosilicate anions. *J. Phys. Chem.* **93**, 1741–1744.

McMillan, G.K., 1991. Understand some basic truths of pH measurement. *Chem. Eng. Prog.* **87** (10), 33–37.

McMillan, G.K., 1993. pH measurement: The state of the art. *Intech* **40** (2), 35–39.

Milliken, T.H., 1950. The chemical characteristics and structure of cracking catalysts. *Discuss. Faraday Soc.* **8**, 279–290.

North, M.R., Swaddle, T.W., 2000. Kinetics of silicate exchange in alkaline aluminosilicate solutions. *Inorg. Chem.* **39**, 2661–2665.

Nyman, M., Krumhansl, J.L., Zhang, P., Anderson, H., Nenoff, T.M., 2000. Chemical evolution of leaked high-level liquid wastes in Hanford soils. *Mater. Res. Soc. Symp. Proc.* **608**, 225–230.

Oelkers, E.H., Schott, J., Devidal, J.L., 1994. The effect of aluminum, pH, and chemical affinity on the rates of aluminosilicate dissolution reaction. *Geochim. Cosmochim. Acta* **58**, 2011–2024.

Papelis, C., Hayes, K.F., Leckie, J.O., 1988. HYDRAQL: a program for the computation of chemical equilibrium composition of aqueous batch systems including surface complexation modeling of ion adsorption at the oxide/solution interface. Stanford, California, Stanford University Technical Report No. 306, 130 pp.

Pitzer, K.S., 1991. Ion interaction approach: Theory and data correlation. In: Pitzer, K.S. (Ed.), *Activity Coefficients in Electrolyte Solutions*, 2nd ed. CRC, Boca Raton, pp. 435–490.

Qafoku, N.P., Ainsworth, C.C., Szecsody, J.E., Qafoku, O.S., Heald, S.M., 2003. Effect of coiupled dissolution and redox reactions on Cr(VI)(aq) attenuation during transport in the sediments under hyperalkaline conditions. *Environ. Sci. Technol.* **37**, 3640–3646.

Qafoku, N.P., Ainsworth, C.C., Szecsody, J.E., Qafoku, O.S., 2004. Transport-controlled kinetic sof dissolution and precipitation in the sediments under alkaline and saline conditions. *Geochim. Cosmochim. Acta* **68**, 2981–2995.

Rasband, W.S., Bright, D.S., 1995. NIH Image—a public domain image-processing program for the Macintosh. *Microbeam Anal.* **4**, 137–149.

Samson, S.D., Nagy, K.L., Cotton, W.B., 2005. Transient and quasi-steady-state dissolution of biotite at22-25 °C in high pH, sodium, nitrate, and aluminate solutions. *Geochim. Cosmochim. Acta* **69**, 399–413.

Sasaki, B., 1962. The corrosive action of aqueous solutions of several electrolytes on the silicic solid surfaces. *Bulletin of the Chemical Research Institute of Non-Aqueous Solutions Tohoku University* **2**, 113–129.

Schindler, P., Kamber, H.R., 1968. Die Acidität von Silanolgruppen. *Helv. Chim. Acta* **51**, 1781–1786.

Schindler, P., Stumm, W., 1987. The surface chemistry of oxides, hydroxides and oxide minerals. In: Stumm, W. (Ed.), *Aquatic Surface Chemistry*. Wiley, New York, pp. 83–110.

Schwartzentruber, J., Fürst, W., Renon, H., 1987. Dissolution of quartz into dilute alkaline solutions at 90 °C: a kinetic study. *Geochim. Cosmochim. Acta* **51**, 1867–1874.

Sjöberg, S., Öhmann, L.O., Ingri, N., 1985. Equilibrium and structural studies of silicon(IV) and aluminum(III) in aqueous-solution. II. Polysilicate formation in alkaline aqueous-solution—A combined potentiometric and Si-29 NMR-study. *Acta Chem. Scand. A Phys. Inorg. Chem.* **39**, 93–107.

Stumm, W., Morgan, J.J., 1996. *Aquatic Chemistry*, 3rd ed. Wiley, New York.

Tester, J.W., Worley, W.G., Robinson, B.A., Grigsby, C.O., Feerer, J.L., 1994. Correlating quartz dissolution kinetics in pure water from 25 to 625 °C. *Geochim. Cosmochim. Acta* **58**, 2407–2420.

Van Bennekom, A.J., Buma, A.G.J., Nolting, R.F., 1991. Dissolved aluminium in the Weddell-Scotia Confluence and effect of Al on the dissolution kinetics of biogenic silica. *Mar. Chem.* **35**, 423–434.

Van Cappellen, P., Qiu, L., 1997a. Biogenic silica dissolution in sediments of the Southern Ocean. I. Solubility. *Deep-Sea Res. II* **44**, 1109–1128.

Van Cappellen, P., Qiu, L., 1997b. Biogenic silica dissolution in sediments of the Southern OceanII Kinetics. *Deep-Sea Res. II* **44**, 1129–1149.

Wan, J.M., Larsen, J.T., Tokunaga, T.K., Zheng, Z.P., 2004. pH neutralization and zonation in alkaline-saline tank waste plumes. *Environ. Sci. Technol.* **38**, 1321–1329.

Wanner, H., Forest, I. (Eds.), 1992. *Chemical Thermodynamics of Uranium*. North-Holland, Amsterdam.

Wesolowski, D.J., 1992. Aluminum speciation and equilibrium in aqueous solution: I. The solubility of gibbsite in the system Na–K–Cl–OH–$Al(OH)_4$ from 0 to 100 °C. *Geochim. Cosmochim. Acta* **56**, 1065–1091.

Wirth, G., Gieskes, J., 1979. The initial kinetics of dissolution of vitreous silica in aqueous media. *J. Colloid Interface Sci.* **68**, 492–500.

Xiao, Y., Lasaga, A.C., 1996. Ab initio quantum mechanical studies of the kinetics and mechanisms of quartz dissolution: OH^- catalysis. *Geochim. Cosmochim. Acta* **60**, 2283–2295.

Zachara, J.M., Ainsworth, C.C., Brown, G.E., Catalano, J.G., McKinely, J.P., Qafoku, O., Smith, S.C., Szecsody, J.E., Traina, S.J., Warner, J.A., 2004. Chromium speciation and mobility in a high level nuclear waste vadose zone plume. *Geochim. Cosmochim. Acta* **68**, 13–30.

Zhao, H.T., Deng, Y.J., Harsh, J.B., Flury, M., Boyle, J.S., 2004. alteration of kaolinite to cancrinite and sodalite by simulated Hanford tank waste and its impact on cesium retention. *Clays Clay Miner.* **52**, 1–13.

Zhuang, J., Flury, M., Jin, Y., 2003. Colloid-facilitated Cs transport through water-saturated Hanford sediment and Ottawa sand. *Environ. Sci. Technol.* **37**, 4905–4911.